Regulation of Protein Function: Crystal Packing Interfaces and Conformational Dimerization[†,‡]

Peter B. Crowley,[*,§] Pedro M. Matias,[||] Hualing Mi,[⊥] Susan J. Firbank,[#] Mark J. Banfield,[#] and Christopher Dennison[#]

UCD School of Biomolecular and Biomedical Science, Conway Institute, University College Dublin, Belfield, Dublin 4, Ireland, Instituto de Tecnologia Química e Biológica, Universidade Nova de Lisboa, Av. Da República, Apartado 127, 2781 901 Oeiras, Portugal, National Laboratory of Plant Molecular Genetics, Institute of Plant Physiology and Ecology, Shanghai Institutes for Biological Sciences, Graduate School of the Chinese Academy of Sciences, 300 Fenglin Road, Shanghai 200032, China, and Institute for Cell and Molecular Biosciences, Medical School, Newcastle University, Newcastle upon Tyne NE2 4HH, U.K.

Received January 22, 2008; Revised Manuscript Received April 18, 2008

ABSTRACT: The accepted view of interprotein electron transport involves molecules diffusing between donor and acceptor redox sites. An emerging alternative hypothesis is that efficient long-range electron transport can be achieved through proteins arranged in supramolecular assemblies. In this study, we have investigated the crystal packing interfaces in three crystal forms of plastocyanin, an integral component of the photosynthetic electron transport chain, and discuss their potential relevance to in vivo supramolecular assemblies. Symmetry-related protein chains within these crystals have Cu−Cu separations of <25 Å, a distance that readily supports electron transfer. In one structure, the plastocyanin molecule exists in two forms in which a backbone displacement coupled with side chain rearrangements enables the modulation of protein−protein interfaces.

Self-assembly is a factor contributing to the molecular organization that maintains the living cell (*1*). For instance, Srere and others have proposed that the formation of supramolecular assemblies is central to the function and regulation of metabolic enzymes (*2* and references therein). Protein recognition and quaternary structure are mediated by the protein surface, which is characterized by a high degree of geometric and chemical complexity. How this surface information is processed (as interprotein contacts) depends on the function of the protein−protein complex, and interface architectures have evolved to confer a broad range of binding affinities and specificities. At the low-affinity extreme are the transient complexes (rate of dissociation of $\sim 10^3$ s^{-1}) such as those formed by redox proteins (*3*). The current model of biological electronic circuitry is based on freely diffusing redox carriers, which bind pseudospecifically (via broadly complementary surface patches) to donor and acceptor redox partners (*3, 4*). However, this model apparently ignores the crowded nature of the intracellular environment (*2, 5, 6*). Given that the macromolecular content of the cell is ~300 g/L (*6*), it is unlikely that proteins diffuse freely over long distances. Macromolecular crowding enhances protein−protein interactions, and therefore, the tendency of a protein will be to form complexes or, in the case of proteins present at high concentrations, to oligomerize in vivo (*5, 6*).

The cupredoxins are one class of electron transporters, which have been subjected to detailed mechanistic and structural studies (*7–10*). Cupredoxins are well-suited to the task of intermolecular electron transfer as their β-sandwich fold typically supports (i) a hydrophobic surface patch surrounding an exposed His ligand of the type 1 copper site and (ii) a collar or cluster of charged side chains (*7*). In vitro kinetic studies demonstrate that the charged patch supports long-range electrostatic interactions with regions of complementary charge on the partner proteins (electrostatic steering), thus enhancing the rate of association (*9, 11–13*). The hydrophobic patch presents a small flat binding site, which facilitates transient pseudospecific interactions (*14, 15*). These attributes of a protein interface are thought to be generally important for transient protein interactions, and a well-studied example is that involving the photosynthetic cupredoxin plastocyanin (Pc)[1] and its partner cytochrome *f* (cyt *f*) (*16, 17*). Interestingly, while numerous in vitro studies have identified charged surfaces as being important for association, in vivo experiments of basic patch mutants of cyt *f* in *Chlamydomonas reinhardtii* have shown that the electrostatic contribution to complex formation is much smaller than expected from the in vitro studies (*18*).

Certain conditions employed for protein crystallization, namely, ~10 mg/mL protein solutions containing high

[†] We thank University College Dublin and Newcastle University for funding. M.J.B. is a Royal Society (UK) University Research Fellow.
[‡] Coordinates have been deposited as Protein Data Bank (PDB) entries 3cvb, 3cvc, and 3cvd.
* To whom correspondence should be addressed. E-mail: peter.crowley@ucd.ie. Telephone: +353 1 716 6711. Fax: +353 1 716 6701.
[§] University College Dublin.
[||] Universidade Nova de Lisboa.
[⊥] Graduate School of the Chinese Academy of Sciences.
[#] Newcastle University.

[1] Abbreviations: cyt *f*, cytochrome *f*; Pc, plastocyanin; PEG, poly(ethylene glycol); rmsd, root-mean-square deviation; WT, wild type.

10.1021/bi800125h CCC: $40.75
Published on Web 05/15/2008

concentrations of poly(ethylene glycol) (PEG), are a good approximation of the crowded environment of the cell (*6*). Moreover, the fact that crystalline samples of redox proteins are capable of rapid interprotein electron transfer (*19–23*) suggests that supramolecular assemblies of redox carriers might act as electronic wires in vivo. The analysis of different crystal forms of the same protein has played an important role in structure−function studies (*24, 25*). Here we describe the structures of three crystal forms of the Leu14Phe hydrophobic patch mutant of Pc from *Phormidium laminosum*. All three crystals were obtained using the same precipitant, in the presence of different metal ions, including the physiologically relevant Mg^{2+}. The L14F mutant was chosen as it has been shown previously that the introduction of a Phe residue into the hydrophobic patch of amicyanin results in dimer formation (*26*). The crystal packing assemblies of Pc are discussed in terms of their possible role in long-range electron transport. In addition, one of the structures provides a notable example of "conformational dimerization" in which the two protein chains exhibit different backbone conformations (*27*).

MATERIALS AND METHODS

Protein Production. The QuikChange method was used to introduce the L14F mutation into a pET11d vector containing the gene for *P. laminosum* Pc (*28*). The resulting plasmid (with the presence of the mutation confirmed by sequencing) was transformed into *Escherichia coli* BL21(DE3) cells for protein expression. Protein purification was performed as described previously (*12, 16*), and the oxidized (blue) protein was exchanged into deionized water for storage.

Protein Crystallization. All of the crystallization trials employed the sitting drop vapor diffusion method. Crystals of L14F Pc were obtained in a range of conditions using a 10 mg/mL protein solution mixed in a 1:1 ratio with (A) 10% PEG 8000, (B) 15% PEG 8000 and 0.2 M $MgCl_2$, and (C) 10% PEG 8000 and 0.2 M zinc acetate. In all cases, the buffer was 0.1 M sodium cacodylate (pH 6.5). The crystals obtained from sample A grew at 32 °C and were colorless, indicating that reduction of the copper occurred during crystal growth. The crystals in samples B and C grew at 21 °C and remained oxidized. Prior to data collection, the crystals in sample C were transferred to a new drop containing the same precipitant but at a lower pH [0.1 M sodium cacodylate (pH 5.1)] supplemented with the reducing agent sodium ascorbate (0.1 mM). Upon reduction, the crystals became colorless.

X-ray Data Collection. Crystals of L14F Pc were flash-frozen in liquid nitrogen using the reservoir solution supplemented with 20% glycerol as the cryoprotectant. Diffraction data were collected using X-rays from an in-house Bruker-Nonius FR-591 generator with a MAR Research 300 mm image plate and on European Synchrotron Radiation Facility beamline ID14-2. The data were processed and reduced with the HKL program package (*29*). Data collection and refinement statistics are given in Table 1.

Structure Solution and Refinement. Initial phases for each crystal structure were obtained by molecular replacement using AMoRe (*31*) and the coordinates of wild-type (WT) *P. laminosum* Pc [PDB entry 1baw (*32*)] as a search model. The asymmetric unit of the crystals obtained from (A) 10% PEG 8000, (B) 15% PEG 8000 and 0.2 M $MgCl_2$, and (C) 10% PEG 8000 and 0.2 M zinc acetate was found to contain two, one, or three protein chains, respectively. Structure refinement and manual rebuilding were performed using REFMAC [as implemented in CCP4 (*33*)] and COOT (*34*), respectively. In the final stages of refinement, hydrogen atoms were added at riding positions and anisotropic *B* factors were refined for each model while monitoring the R_{factor} and R_{free} values. Crystal packing interfaces were analyzed using PISA (*35*); the C-alpha matching program (*36*) was used to superpose the different structures, and protein structure figures were generated with PYMOL (http://www.pymol.org).

Protein Data Bank Entries. Crystallographic coordinates for the three structures [Monomer (3cvc), Dimer (3cvb), and Trimer (3cvd)] have been deposited in the PDB.

RESULTS AND DISCUSSION

Crystal Structure Overview. The crystallization conditions, data collection statistics, and refinement statistics for the three L14F Pc structures are summarized in Table 1. The refined models of the asymmetric units comprise one protein chain ($P2_12_12_1$ form), two protein chains ($P2_1$ form), and three protein chains ($P4_32_12$ form); for convenience, these structures are termed Monomer, Dimer, and Trimer, respectively. Continuous electron density was present for all chains in the Monomer and Dimer structures for residues Glu1−Gly105; in the Trimer structure, there was insufficient electron density to model Gly105. In the Dimer structure, the loop between Ser77 and Phe80 in chain A is modeled at 70% occupancy. The electron density in this region displays features that could be consistent with other conformations for this loop, but a discrete alternative structure could not be satisfactorily modeled. Alternate conformations were modeled for several side chains, while the electron density was incomplete for various surface-exposed side chains.

In all of the structures, each protein chain binds a Cu atom at a type 1 copper site, with ligands to the metal provided by the side chains of His39, Cys89, His92, and Met97. In addition to the Cu site, the Monomer structure has a $[Mg(H_2O)_6]^{2+}$ complex bound at a crystal interface and the Trimer structure has four Zn^{2+} ions (one modeled at half-occupancy). Finally, residual electron density is present in the region of Glu70 in each of the molecules in the Trimer structure. This density cannot be attributed to any compound to which the protein was exposed during purification or crystallization and therefore has not been modeled.

Crystal Packing Interfaces and Conformation Changes. In terms of "global" conformation changes, it appears that at the physiologically relevant ionic strength of 0.1 M sodium cacodylate (pH 6.5), crystal growth proceeds via formation of weak dimer interfaces. When the ionic strength is increased by the addition of 0.2 M $MgCl_2$, the protein packs as a monomer, and when Mg^{2+} is replaced with Zn^{2+}, the protein forms zinc-mediated trimers. Note that none of the crystal packing interfaces (Table 2) involve the L14F site, and therefore, similar results are expected for WT Pc [which crystallizes as a trimer in the presence of Zn^{2+}, 1baw, 2.8 Å resolution (*32*)]. Clearly, the three crystallization conditions influence the protein−protein interactions and thus give rise to substantially different crystal packing environments. To facilitate the different packing environments, the protein must

Table 1: Summary of Crystallization Conditions, Data Collection Statistics, and Refinement Statistics of Leu14Phe Pc Structures

	Monomer[a] [Cu(II)]	Dimer[a] [Cu(I)]	Trimer[a] [Cu(I)]
Crystallization Conditions[b]			
% poly(ethylene glycol) 8000	15	10	10
salt	0.2 M $MgCl_2$	−	0.2 M zinc acetate
Data Collection			
diffraction radiation source	FR-591 rotating anode	ESRF ID14-2	ESRF ID14-2
detector	MAR research MAR 300	ADSC Quantum 4	ADSC Quantum 4
wavelength (Å)	1.5418	0.933	0.933
space group	$P2_12_12_1$	$P2_1$	$P4_32_12$
resolution range (Å)	21.11−1.72 (1.81−1.72)	33.7−1.40 (1.48−1.40)	29.3−1.50 (1.58−1.50)
cell constants	$a = 23.9$ Å $b = 55.5$ Å $c = 65.0$ Å $\alpha = \beta = \gamma = 90°$	$a = 33.7$ Å $b = 33.4$ Å $c = 78.5$ Å $\alpha = \gamma = 90°$, $\beta = 90.55°$	$a = b = 85.8$ Å $c = 90.3$ Å $\alpha = \beta = \gamma = 90°$
no. of unique reflections	9680	34119	54990
multiplicity	3.2 (3.2)[c]	3.4 (2.5)[c]	6.6 (5.9)[c]
$I/\sigma(I)$	24.0 (9.1)[c]	23.4 (8.1)[c]	22.2 (3.8)[c]
completeness (%)	99.3 (98.9)[c]	98.2 (88.2)[c]	100.0 (99.9)[c]
R_{merge}[d] (%)	3.7 (12.6)[c]	3.7 (8.8)[c]	5.2 (35.7)[c]
solvent content (%)	32.9	34.3	47.6
Refinement			
R_{factor} (%)	13.4 (12.7)[c]	12.5 (9.6)[c]	15.2 (14.2)[c]
R_{free} (%)	19.2 (23.7)[c]	17.2 (18.0)[c]	18.3 (20.0)[c]
rmsd[e] for bonds (Å)/ rmsd for angles (deg)	0.013/1.41	0.015/1.59	0.015/1.58
mean positional error (Å)	0.07	0.03	0.04
average B factor for protein/ligands (Å^2)	10.1/22.6	10.1/23.7	18.2/32.5
no. of non-hydrogen atoms	988	1933	2950
no. of copper atoms	1	2	3
no. of zinc atoms	−	−	3.5
no. of water molecules	179	328	507
Ramachandran analysis (all chains)[f]			
% residues in favored regions	98.1	98.6	97.9
% residues in allowed regions	100.0	100.0	100.0

[a] The name of the data set refers to the number of Pc molecules that make up the asymmetric unit. [b] The buffer was 0.1 M sodium cacodylate (pH 6.5). Data collection for the trimer structure was performed using a crystal soaked in 0.1 M sodium cacodylate (pH 5.1). [c] Values in parentheses correspond to those for the highest-resolution shell. [d] $R_{merge} = \sum_h\sum_i|I_i(hkl) - \langle I(hkl)\rangle|/\sum_h\sum_i I_i(hkl)$. [e] Root-mean-square deviation of temperature factors of bonded atoms. [f] Calculated in MOLPROBITY (*30*).

Table 2: Properties of Leu14Phe Pc Crystal Packing Interfaces[a]

			interface properties		
crystal	space group	symmetry operation	size (Å^2)[b]	% apolar	no. of hydrogen bonds
Monomer	$P2_12_12_1$	$x - 1, y, z$	270	64	2
Dimer[c]	$P2_1$	(1) A−B $-x + 1, y - {}^1/_2, -z$	310	52	4
		(2) A−B $-x, y - {}^1/_2, -z$	270	62	2
		(3) B−B $-x + 1, y - {}^1/_2, -z - 1$	280	69	0
		(4) A−A $-x, y - {}^1/_2, -z$	250	82	0
Trimer[d]	$P4_32_12$	x, y, z	330	46	9

[a] Only the largest interfaces, which bury ≥250 Å^2 of surface area per chain, are listed. [b] Interface size is given as the loss in surface accessibility per chain. [c] The chain identifiers (A and B) are indicated. See Figure 3 for a comparison of interfaces 1 and 2. The A−B interface found in the asymmetric unit buries 120 Å^2 of surface area per chain. [d] The values listed are the average properties for the three Zn-mediated interfaces. Note that the A−B, B−C, and C−A interfaces are equivalent due to the 3-fold symmetry of the trimer and each chain buries 2 × 330 Å^2 of surface area and forms 2 × 9 hydrogen bonds. All other crystal contacts involve surface areas of <200 Å^2.

undergo numerous small conformation changes. In addition to side chain reorganization and altered hydrogen bonding patterns, the flexible loop regions are prone to conformation changes. Information about the crystal packing interfaces was obtained using PISA (*35*), and the properties of the interfaces (which bury ≥250 Å^2 of surface area per chain) are listed in Table 2.

A detailed analysis of the conformation changes associated with crystal packing was performed by first superposing the protein chains (a total of six chains from three structures) and calculating the root-mean-square deviations (rmsds) for the C$^\alpha$ atoms. For the purposes of comparison, the Monomer structure was used as a reference and the individual chains from the Dimer and Trimer structures were superposed. Figure 1 is a plot of the rmsds for the C$^\alpha$ positions. The average rmsd between the Monomer structure and the other chains varied over the range of 0.3−0.5 Å. As one might expect, the relatively flexible α-helical and loop regions show large deviations and a similar pattern is found for the C$^\alpha$ temperature factors (Figure S1, Supporting Information). The extent of the rmsd depends on the degree to which the loops are engaged in interface formation. For instance, in the Trimer structure, particularly large conformation changes are observed for Asp44 and Asp45 which rearrange to bind an interfacial zinc ion. The loop region of Ser77−Phe80 shows a spread of rmsd values pointing to different conformations within the Trimer. Significant effects are also observed around Arg93, which will be discussed below.

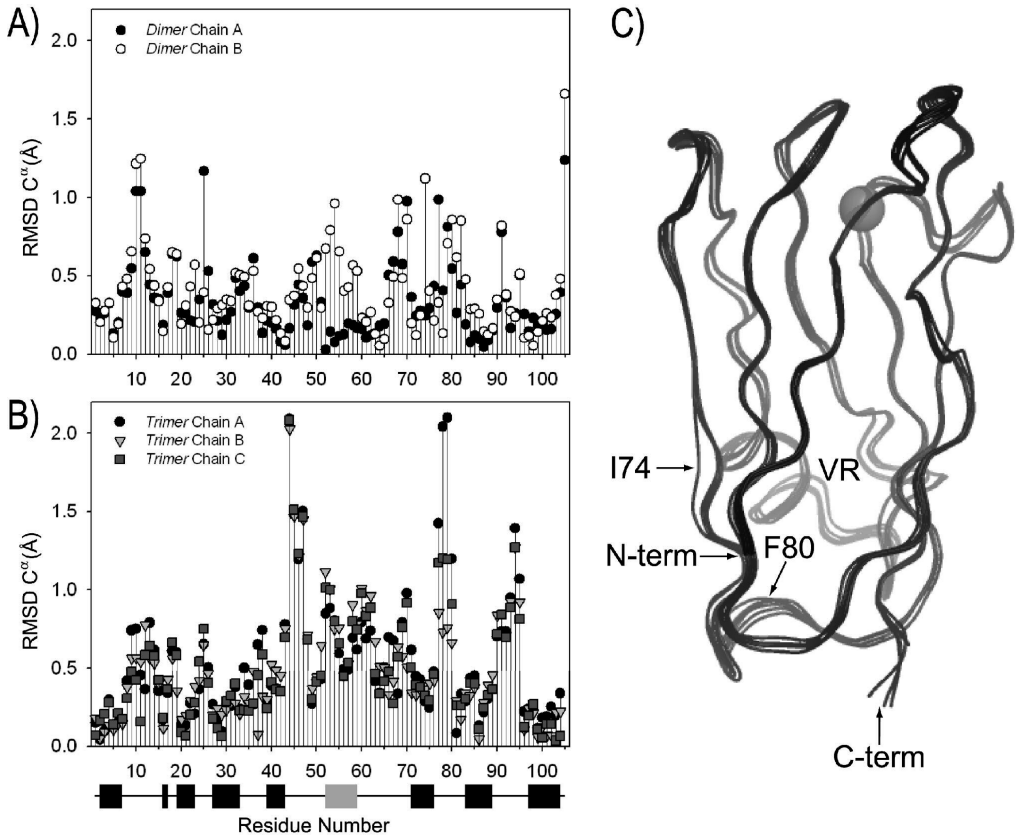

FIGURE 1: Root-mean-square deviation (rmsd) of the positions of the C^{α} atoms in (A) Dimer and (B) Trimer structures with respect to the Monomer structure. Regions of β-strand and α-helical secondary structure are identified by the black and gray boxes, respectively (below panel B). (C) Superposition of the C^{α} traces for all six chains from the Monomer, Dimer, and Trimer structures. In this orientation, the variable region of Pc (residues 44−60, labeled VR) which includes an α-helix is toward the back of the molecule. The copper ion is represented as a gray sphere. The large rmsd for the C^{α} atom of Ile74 in Dimer chain B is apparent (see also panel A).

Conformational Dimerization. In contrast to the loops, the majority of the C^{α} atoms located in β-strands have small (<0.5 Å) rmsd values (Figure 1) and low *B* factors (Figure S1, Supporting Information). In other words, the β-sandwich structure is well-preserved in the different crystal forms. The one exception is Ile74 in Dimer chain B (Figure 1) which deviates by 1.2 Å from its position in chain A, a surprising result considering the rigidity of the cupredoxin fold (*37*). Given the high resolution of these structures, such a deviation is significant. Both of the interstrand hydrogen bonds between Ile74 and Val29 increase in length by 0.1 Å compared to those in chain A. The backbone conformation change is likely driven by the rotation of Ile74 (~120° about the $C^{\alpha}-C^{\beta}$ bond) which results in the $C^{\delta 1}$ atom being surface-exposed in chain B (Figure 2). Accompanying this rotation are significant conformation changes of the buried side chains of both Leu59 and Phe80 in the immediate vicinity of Ile74. The structural differences between Dimer chains A and B have interesting consequences for crystal packing interfaces, the largest of which form around Ile74 (Table 2 and Figure 2). Despite involving identical regions of the protein, the superposition of the two dimers reveals that the side chain packing at the interfaces is strikingly different (Figure 2). The backbone conformation change facilitates a closer association of the two chains, resulting in a slightly larger interface. In particular, the flipped side chain of Ile74-B makes van der Waals contact with the C^{β} atom of Ala51-A, whereas the equivalent region of the smaller, "loose" interface contains three ordered water molecules. In addition, two interfacial hydrogen bonds between the side chains of

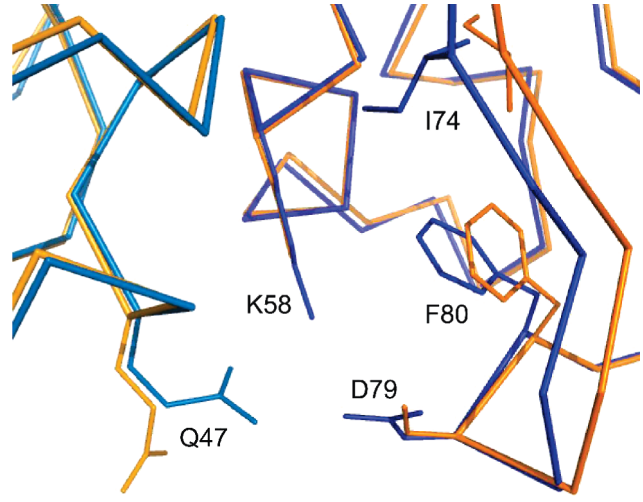

FIGURE 2: Structural superposition of the crystal packing interfaces of chain A (orange) and chain B (blue) in the Dimer structure. The symmetry operation $-x$, $y - {}^{1}/_{2}$, $-z$ relates the light and dark orange chains, whereas the light and dark blue chains are related by $-x + 1$, $y - {}^{1}/_{2}$, $-z$. Despite involving identical regions of the protein, the side chain packing at the two interfaces is strikingly different on account of the rotation of Ile74 (chain B, see also Figure 1C). The larger interface (in blue) arises from a closer association of the two chains, hence the large "positional" rmsd between the dark blue and orange chains (see the text for further details).

Gln47-A, Lys58-B, and Asp79-B are absent from the loose interface. In the latter, the side chain amide of Gln47-B is rotated away from the interface and the absence of complete electron density for Lys58-A and Asp79-A indicates that this

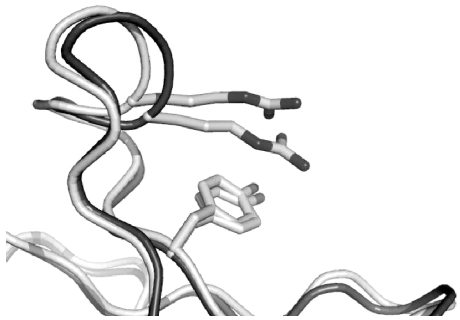

FIGURE 3: Structural superposition of part of the C^{α} backbone of the Monomer (dark gray) and Trimer chain A illustrates conformation changes due to the different crystal packing environments. The intramolecular cation$-\pi$ interaction between Arg93 and Tyr88 is weakened in the Trimer as a consequence of intermolecular interactions.

interface is more loosely packed. In fact, the loop region of Ser77−Phe80 in chain A is highly flexible, and the data here are best described by modeling at 70% occupancy for the backbone and side chain atoms. Additional contacts between this loop and chain B (via a separate crystal packing interface burying ~100 Å^2 per chain) involve the Ala9−Gly12 loop of the latter. Although the differences are small, the temperature factor plots (Figure S1, Supporting Information) reveal that the *B* factors are higher for chain A residues Ser77−Phe80 and chain B residues Ala9−Gly12 than for the equivalent Ser77−Phe80 region of chain B and the neighboring Ala9−Gly12 loop of chain A, which are more rigid. The other pair of symmetry-related interfaces (Table 2) have a high hydrophobic content due to the participation of Phe66 and Pro68 and exhibit minor differences.

Therefore, it appears that the crystallization conditions, which support dimerization, give rise to two subtly different forms of Pc, thus enabling modulation of protein−protein interactions. In particular, the data suggest that the interface tightness (the degree of atom packing) can be tuned. Presumably, the increased affinity of the larger interface sufficiently outweighs any energy cost involved in the conformation change. Given that Ile74 belongs to a strand on the edge of the β-sheet it is more amenable to a change in conformation. Interestingly, conformational dimerization has been shown to play an important role in the oligomerization of Mad2, which exists in open and closed conformations that differ in the location of two β-strands. It is suspected that dimerization facilitates conversion from the open to the closed form and thus regulates binding of the closed form to partner proteins (*27*).

Polar Interactions. Protein crystal packing interfaces have, on average, one hydrogen bond per ~140 Å^2 of buried surface area (*38*). Counting all of the hydrogen bonds between each individual protein chain and all crystal packing neighbors in the Pc structures reveals that each chain makes 10−18 intermolecular hydrogen bonds. The number of hydrogen bonds increases as follows: Dimer < Monomer < Trimer. Table 2 highlights the distribution of hydrogen bonds in the different interfaces. The differences in hydrogen bonding for interfaces 1 and 2 in the Dimer structure have been discussed above. The Trimer interface stands out as having an exceptionally high density of hydrogen bonds (18 per chain). This is partly explained by the fact that the Trimer interface contains more polar groups than the interfaces found in the Monomer and Dimer structures. Such charge-rich interfaces are considered unfavorable as energy is required to desolvate the charged groups (*39*). However, in the Trimer structure, coordination of the bridging zinc ion [by the imidazole of His61 and the carboxylates of Asp44 (as a bidentate ligand) and Asp45 (monodentate) from the neighboring monomer] is energy-releasing and therefore compensates (at least in part) for desolvation effects.

When considering the effect of protein−protein interfaces on polar interactions, an interesting case involves Arg93 (conserved in cyanobacterial Pcs) and Tyr88 (conserved in almost all Pc sequences). In the Monomer and Dimer structures, the side chains of Arg93 and Tyr88 make several hydrogen bonds to water molecules, while the guanidinium group and the aromatic ring pack in a coplanar fashion (3.4−3.6 Å separation) to yield an energetically favorable cation$-\pi$ interaction (*40, 41*) (Figure 3). In the Trimer structure, Arg93 and Tyr88 are located in the Zn-mediated interface and form intermolecular hydrogen bonds with neighboring molecules. The packing of the two side chains is no longer coplanar; the separation distance increases to 4.1−4.9 Å (see Figure 3), and the cation$-\pi$ interaction is considerably weakened. Therefore, the intramolecular cation$-\pi$ interaction is attenuated in favor of intermolecular interactions.

Crystal Packing and Implications for Regulation of Pc Function. Photosynthetic electron transport between cytochrome *bf* and photosystem I is maintained by Pc, and numerous studies have explored Pc function in the context of diffusion in the thylakoid lumen (*42–45*). The narrow confines of the thylakoid lumen and the abundance of large membrane-bound proteins are expected to severely impede the motion of Pc (*42, 44*). In addition, the electrostatic contribution to fast interprotein electron transfer observed in vitro is considerably dampened in vivo (*18*), yet long-range electron transport is not rate-limiting. While particular structural features pertinent to Pc function have been identified (*7, 9, 12, 17*), how function is regulated remains unclear. On one hand, it has been shown that the concentration of Pc in the thylakoid lumen increases linearly with increasing flux rates of electron transport (*45*). On the other hand, acidification of the lumen has been suggested as a potential downregulator of Pc function, since the exposed His ligand of reduced Pc dissociates from the cuprous site to become protonated at low pH (*46*). Regulation can also be achieved at the level of protein−protein interactions. Given the high protein concentration (>20 mg/mL) (*47*) and the constricted volume of the thylakoid lumen (*42*), photosynthetic electron transport is subject to macromolecular crowding effects (*5, 6*). In particular, as one of the most abundant proteins in the thylakoid (*47*), Pc will have a strong propensity to form oligomers. Previously, we proposed that rather than achieving electron transport via the net displacement of one Pc molecule, transport could involve electron hopping between neighboring Pc molecules (*15*). Such a mechanism, which relies on electron self-exchange (*9, 10, 15, 48*), is analogous to the Grotthus mechanism for proton transport in water and eliminates the necessity for long-range protein diffusion.

The existence of ordered protein assemblies, including protein crystals, in vivo is well-documented (reviewed in ref *49*). For example, the growth of spinach under low-light conditions results in semicrystalline arrays of photosystem II (*50*). This supramolecular organization of the photosystem is thought to be necessary to ensure that diffusion of plastoquinone is not rate-limiting. The Dimer structure was

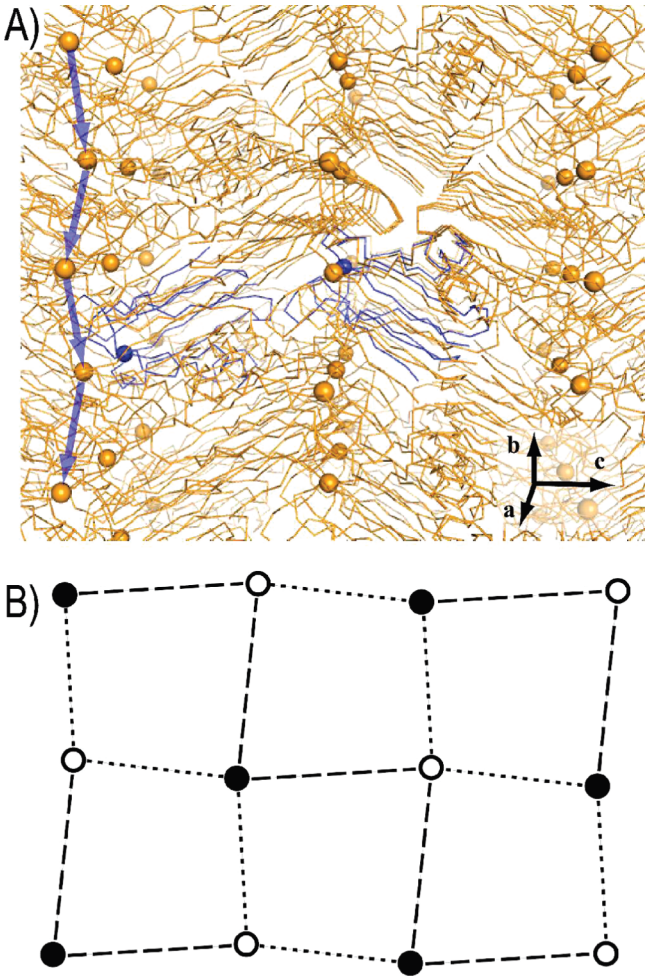

FIGURE 4: Symmetry-related crystal packing neighbors in the Dimer structure (space group $P2_1$). (A) The two protein molecules of the asymmetric unit are shown as blue C^{α} traces with the copper ions depicted as blue spheres, while symmetry-related neighbors are colored orange. The orientation of the unit cell is indicated. Blue arrows highlight the most probable (shortest distance) electron transfer pathway between neighboring monomers. (B) A plane of copper ions with the copper−copper distances denoted by the dotted (22.0 Å) and dashed (25.6 Å) lines. The dotted lines correspond to the blue arrows in (A). Filled and empty circles indicate the up and down orientations, respectively, of the plastocyanin molecules.

grown from crystallization conditions (10 mg/mL protein with 10% PEG 8000), which provide a good approximation of macromolecular crowding in the cell (*6*). Therefore, the crystal packing interfaces in the Dimer may be reminiscent of protein interactions that contribute to supramolecular assemblies in vivo. With a solvent content as low as 34%, the protein molecules in this structure are tightly packed. While the Cu−Cu separation between the two molecules of the asymmetric unit is long (~40 Å), symmetry-related molecules form planes of redox centers with the shortest Cu−Cu separation being 22 Å (Figure 4). This distance is suitable for long-range electron transfer (*19–23*), though the intermolecular arrangement is distinct from that which is thought to be involved in electron self-exchange (*9, 10, 15, 48*). To form the Dimer structure, Pc exists in two different conformations, involving a 1.2 Å displacement of a β-strand, which suggests that under the constraints of macromolecular crowding even the compact cupredoxin fold is prone to reorganization. In the Monomer structure, symmetry-related proteins are again amenable to interprotein electron transfer with a Cu−Cu separation of 24 Å. In the Trimer structure, Zn^{2+} ions mediate the protein−protein contacts, but without knowledge of the zinc availability in the thylakoid, it is debatable whether this structure is physiologically relevant. However, it is worth noting that insulin is stored in a crystalline form (in pancreatic β-cells), which requires the presence of zinc (*50*).

To summarize, Pc occurs in the thylakoid lumen where it is subject to macromolecular crowding effects (high protein concentration, constricted lumenal volume). With high flux rates, the concentration of Pc is increased to meet the demand of photosynthetic electron transport (*45*), and this increase in concentration may promote the formation of ordered Pc assemblies. Working from the premise that crystallization conditions, such as highly concentrated poly(ethylene glycol) solutions, mimic the crowded environment in the cell (*6*), we suggest that crystal packing arrangements could be physiologically relevant (*19*). Given that the observed Cu−Cu distances (Figure 4) are suited to long-range electron transfer (*19*), it seems plausible to suggest that Pc self-assembly is a factor contributing to the electronic circuitry of photosynthesis.

CONCLUSIONS

Three crystal forms of Pc have been described in terms of the potential relevance of crystal packing interfaces to in vivo interactions. While Pc is conventionally viewed as a monomeric protein which diffuses between donor and acceptor redox sites, we propose that efficient long-range electron transport can also be achieved via supramolecular assemblies of Pc. Redox protein crystals could be representative of such assemblies, which may function as electronic wires in the crowded cellular environment. The small size (~35 Å diameter) of Pc ensures that different packing arrangements can be formed, which have short Cu−Cu distances (<25 Å) suitable for electron tunnelling (*19–23*). In addition, we find evidence of conformational dimerization (*27*) in the relatively "minimalist" cupredoxin fold. In the Dimer structure, Pc exists in two forms in which a backbone displacement coupled with side chain rearrangements enables the modulation of protein−protein interfaces.

ACKNOWLEDGMENT

Acknowledged are Prof. P. C. Engel (University College Dublin) for helpful discussions and Prof. M. A. Carrondo (ITQB) for access to research facilities. The European Synchrotron Radiation Facility is acknowledged for access to beamline ID14-2.

SUPPORTING INFORMATION AVAILABLE

A description of the bridging ions and water molecules found in the three structures and plots of the C^{α} temperature (*B*) factors. This material is available free of charge via the Internet at http://pubs.acs.org.

REFERENCES

1. Whitesides, G. M., and Grzybowski, B. (2002) Self-assembly at all scales. *Science 295*, 2418–2421.
2. Srere, P. A. (2000) Macromolecular interactions: Tracing the roots. *Trends Biochem. Sci. 25*, 150–153.
3. Bendall D. S., Ed. (1996) *Protein Electron Transfer*, Bios Scientific, Oxford, U.K.
4. Williams, P. A., Fulop, V., Leung, Y. C., Chan, C., Moir, J. W. B., Howlett, G., Ferguson, S. J., Radford, S. E., and Hajdu, J. (1995) Pseudospecific docking surfaces on electron transfer proteins as

illustrated by pseudoazurin, cytochrome c550 and cytochrome cd1 nitrite reductase. *Nat. Struct. Biol. 2*, 975–982.
5. Ellis, R. J. (2001) Macromolecular crowding: An important but neglected aspect of the intracellular environment. *Curr. Opin. Struct. Biol. 11*, 114–119.
6. Minton, A. P. (2006) How can biochemical reactions within cells differ from those in test tubes? *J. Cell Sci. 119*, 2863–2869.
7. De Rienzo, F., Gabdoulline, R. R., Menzani, M. C., and Wade, R. C. (2000) Blue copper proteins: A comparative analysis of their molecular interaction properties. *Protein Sci. 9*, 1439–1454.
8. Sato, K., Kohzuma, T., and Dennison, C. (2003) Active-site structure and electron-transfer reactivity of plastocyanins. *J. Am. Chem. Soc. 125*, 2101–2112.
9. Dennison, C. (2005) Investigating the structure and function of cupredoxins. *Coord. Chem. Rev. 249*, 3025–3054.
10. Li, C., Yanagisawa, S., Martins, B. M., Messerschmidt, A., Banfield, M. J., and Dennison, C. (2006) Basic requirements for a metal-binding site in a protein: The influence of loop shortening on the cupredoxin azurin. *Proc. Natl. Acad. Sci. U.S.A. 103*, 7258–7263.
11. Kannt, A., Young, S., and Bendall, D. S. (1996) The role of acidic residues of plastocyanin in its interaction with cytochrome f. *Biochim. Biophys. Acta 1277*, 115–126.
12. Schlarb-Ridley, B. G., Bendall, D. S., and Howe, C. J. (2003) Relation between interface properties and kinetics of electron transfer in the interaction of cytochrome f and plastocyanin from plants and the cyanobacterium *Phormidium laminosum*. *Biochemistry 42*, 4057–4063.
13. Sato, K., Kohzuma, T., and Dennison, C. (2004) Pseudospecificity of the acidic patch of plastocyanin for the interaction with cytochrome *f*. *J. Am. Chem. Soc. 126*, 3028–3029.
14. Crowley, P. B., and Carrondo, M. A. (2004) The architecture of the binding site in redox protein complexes: Implications for fast dissociation. *Proteins 55*, 603–612.
15. Sato, K., Crowley, P. B., and Dennison, C. (2005) Transient homodimer interactions studied using the electron self-exchange reaction. *J. Biol. Chem. 280*, 19281–19288.
16. Crowley, P. B., Otting, G., Schlarb-Ridley, B. G., Canters, G. W., and Ubbink, M. (2001) Hydrophobic interactions in a cyanobacterial plastocyanin-cytochrome f complex. *J. Am. Chem. Soc. 123*, 10444–10453.
17. Crowley, P. B., and Ubbink, M. (2003) Close encounters of the transient kind: Protein interactions in the photosynthetic redox chain investigated by NMR spectroscopy. *Acc. Chem. Res. 36*, 723–730.
18. Soriano, G. M., Ponamarev, M. V., Tae, G. S., and Cramer, W. A. (1996) Effect of the interdomain basic region of cytochrome f on its redox reactions in vivo. *Biochemistry 35*, 14590–14598.
19. Tezcan, F. A., Crane, B. A., Winkler, J. R., and Gray, H. B. (2001) Electron tunneling in protein crystals. *Proc. Natl. Acad. Sci. U.S.A. 98*, 5002–5006.
20. Crane, B. R., Di Bilio, A. J., Winkler, J. R., and Gray, H. B. (2001) Electron tunneling in single crystals of *Pseudomonas aeruginosa* azurins. *J. Am. Chem. Soc. 123*, 11623–11631.
21. Guo, M., Bhaskar, B., Li, H., Barrows, T. P., and Poulos, T. L. (2004) Crystal structure and characterization of a cytochrome c peroxidase-cytochrome c site-specific cross-link. *Proc. Natl. Acad. Sci. U.S.A. 101*, 5940–5945.
22. Pearson, A. R., Mozzarelli, A., and Rossi, G. L. (2004) Microspectrophotometry for structural enzymology. *Curr. Opin. Struct. Biol. 14*, 656–662.
23. Kang, S. A., and Crane, B. R. (2005) Effects of interface mutations on association modes and electron-transfer rates between proteins. *Proc. Natl. Acad. Sci. U.S.A. 102*, 15465–15470.
24. Crosio, M. P., Janin, J., and Jullien, M. (1992) Crystal packing in six crystal forms of pancreatic ribonuclease. *J. Mol. Biol. 228*, 243–251.
25. Huang, D. B., Ainsworth, C. F., Stevens, F. J., and Schiffer, M. (1996) Three quaternary structures for a single protein. *Proc. Natl. Acad. Sci. U.S.A. 93*, 7017–7021.
26. Carrell, C. J., Sun, D., Jiang, S., Davidson, V. L., and Mathews, F. S. (2004) Structural studies of two mutants of amicyanin from *Paracoccus denitrificans* that stabilize the reduced state of the copper. *Biochemistry 43*, 9372–9380.
27. Mapelli, M., Filipp, F. V., Rancati, G., Massimiliano, L., Nezi, L., Stier, G., Hagan, R. S., Confalonieri, S., Piatti, S., Sattler, M., and Musacchio, A. (2006) Determinants of conformational dimerization of Mad2 and its inhibition by p31comet. *EMBO J. 25*, 1273–1284.
28. Schlarb, B. G., Wagner, M. J., Vijgenboom, E., Ubbink, M., Bendall, D. S., and Howe, C. J. (1999) Expression of plastocyanin and cytochrome f of the cyanobacterium *Phormidium laminosum* in *Escherichia coli* and *Paracoccus denitrificans* and the role of leader peptides. *Gene 234*, 275–283.
29. Otwinowski, Z., and Minor, W. (1997) Processing of X-ray Diffraction Data Collected in Oscillation Mode. *Methods Enzymol. 276*, 307–326.
30. Lovell, S. C., Davis, I. W., Arendall, W. B., de Bakker, P. I. W., Word, J. M., Prisant, M. G., Richardson, J. S., and Richardson, D. C. (2003) Structure validation by Cα geometry: φ, ψ and Cβ deviation. *Proteins 50*, 437–450.
31. Navaza, J. (1994) AMoRe: an Automated Package for Molecular Replacement. *Acta Crystallogr. A50*, 157–163.
32. Bond, C. S., Bendall, D. S., Freeman, H. C., Guss, J. M., Howe, C. J., Wagner, M. J., and Wilce, M. C. J. (1999) The structure of plastocyanin from the cyanobacterium *Phormidium laminosum*. *Acta Crystallogr. D55*, 414–421.
33. Collaborative Computational Project, Number 4 (1994) The CCP4 suite: Programs for protein crystallography. *Acta Crystallogr. D50*, 760–763.
34. Emsley, P., and Cowtan, K. (2004) Coot: Model-building tools for molecular graphics. *Acta Crystallogr. D60*, 2126–2132.
35. Krissinel, E., and Henrick, K. (2007) Inference of macromolecular assemblies from crystalline state. *J. Mol. Biol. 372*, 774–797.
36. Bachar, O., Fischer, D., Nussinov, R., and Wolfson, H. (1993) A computer vision based technique for 3-D sequence-independent structural comparison of proteins. *Protein Eng. 6*, 279–287.
37. Bertini, I., Bryant, D. A., Ciurli, S., Dikiy, A., Fernandez, C. O., Luchinat, C., Safarov, N., Vila, A. J., and Zhao, J. (2001) Backbone dynamics of plastocyanin in both oxidation states. Solution structure of the reduced form and comparison with the oxidized state. *J. Biol. Chem. 276*, 47217–47226.
38. Bahadur, R. P., Chakrabarti, P., Rodier, F., and Janin, J. (2004) A dissection of specific and non-specific protein-protein interfaces. *J. Mol. Biol. 336*, 943–955.
39. Collins, K. D., and Washabaugh, M. W. (1985) The Hofmeister effect and the behaviour of water at interfaces. *Q. Rev. Biophys. 18*, 323–422.
40. Gallivan, J. P., and Dougherty, D. A. (1999) Cation-π interactions in structural biology. *Proc. Natl. Acad. Sci. U.S.A. 96*, 9459–9464.
41. Crowley, P. B., and Golovin, A. (2005) Cation-π interactions in protein-protein interfaces. *Proteins 59*, 231–239.
42. Whitmarsh, J. (1986) Mobile electron carriers in thylakoids. In *Encyclopedia of Plant Physiology* (Staehlin, L. A., and Arntzen, C. J., Eds.) pp 508, Springer, Berlin.
43. Haehnel, W., Ratajczak, R., and Robenek, H. (1989) Lateral distribution and diffusion of plastocyanin in chloroplast thylakoids. *J. Cell Biol. 108*, 1397–1405.
44. Cruz, J. A., Salbilla, B. A., Kanazawa, A., and Kramer, D. M. (2001) Inhibition of plastocyanin to P700 electron transfer in *Chlamydomonas reinhardtii* by hyperosmotic stress. *Plant Physiol. 127*, 1167–1179.
45. Schottler, M. A., Kirchhoff, H., and Weis, E. (2004) The role of plastocyanin in the adjustment of the photosynthetic electron transport to the carbon metabolism in tobacco. *Plant Physiol. 136*, 4265–4274.
46. Guss, J. M., Harrowell, P. R., Murata, M., Norris, V. A., and Freeman, H. C. (1986) Crystal structure analyses of reduced (Cu I) poplar plastocyanin at six pH values. *J. Mol. Biol. 192*, 361–387.
47. Kieselbach, T., Hagman, Å., Andersson, B., and Schroder, W. P. (1998) The thylakoid lumen of chloroplasts, isolation and characterization. *J. Biol. Chem. 273*, 6710–6716.
48. van Amsterdam, I. M. C., Ubbink, M., Einsle, O., Messerschmidt, A., Merli, A., Cavazzini, D., Rossi, G. L., and Canters, G. W. (2002) Dramatic modulation of electron transfer in protein complexes by crosslinking. *Nat. Struct. Biol. 9*, 48–52.
49. Doye, J. P. K., and Poon, W. C. K. (2006) Protein crystallization in vivo. *Curr. Opin. Colloid Interface Sci. 11*, 40–46.
50. Kirchhoff, H., Haase, W., Wegner, S., Danielsson, R., Ackermann, R., and Albertsson, P. A. (2007) Low-light-induced formation of semi-crystalline photosystem II arrays in higher plant chloroplasts. *Biochemistry 46*, 11169–11176.

BI800125H